AGU Advances

RESEARCH ARTICLE
10.1029/2019AV000103

Yangyang Xu and Xiaokang Wu contributed equally to this work.

Key Points:
- A regional-scale assessment for the present-day heatwave and high-PM occurrence and future changes is presented
- The rare heatwave and high-PM hazards (HHH) would have large increases, in contrast to smaller increases in heatwave or high PM individually
- The alarming increase rate in the next few decades poses great challenges to adaptation, calling for a holistic view of the health impacts

Supporting Information:
- Supporting Information S1
- Original Version of Manuscript
- Peer Review History
- First Revision of Manuscript
- Second Revision of Manuscript [Accepted]

Correspondence to:
Y. Xu,
yangyang.xu@tamu.edu

Citation:
Xu, Y., Wu, X., Kumar, R., Barth, M., Diao, C., Gao, M., et al. (2020). Substantial increase in the joint occurrence and human exposure of heatwave and high-PM hazards over South Asia in the mid-21st century. *AGU Advances*, *1*, e2019AV000103. https://doi.org/10.1029/2019AV000103

Received 16 JUL 2019
Accepted 16 DEC 2019

Peer Review. The peer review history for this article is available as a PDF in the Supporting Information.

Substantial Increase in the Joint Occurrence and Human Exposure of Heatwave and High-PM Hazards Over South Asia in the Mid-21st Century

Yangyang Xu[1], Xiaokang Wu[1,2], Rajesh Kumar[2], Mary Barth[2], Chenrui Diao[1], Meng Gao[3], Lei Lin[4], Bryan Jones[5], and Gerald A. Meehl[2]

[1]Department of Atmospheric Sciences, Texas A&M University, College Station, TX, USA, [2]National Center for Atmospheric Research, Boulder, CO, USA, [3]Department of Geography, Hong Kong Baptist University, Hong Kong, SAR, China, [4]School of Atmospheric Sciences and Guangdong Province Key Laboratory for Climate Change and Natural Disaster Studies, Sun Yat-Sen University, Zhuhai, Guangdong, China, [5]Baruch College, Marxe School of Public and International Affairs, New York, NY, USA

Abstract Extreme heat occurrence worldwide has increased in the past decades. Greenhouse gas emissions, if not abated aggressively, will lead to large increases in frequency and intensity of heat extremes. At the same time, many cities are facing severe air pollution problems featuring high-PM episodes that last from days to weeks. Based on a high-resolution decadal-long model simulation using a state-of-the-science regional chemistry-climate model that is bias corrected against reanalysis, here we show that when daily average wet-bulb temperature of 25 °C is taken as the threshold for severe health impacts, heat extremes frequency averaged over South Asia increases from 45 ± 5 days/year in 1997–2004 to 78 ± 3 days/year in 2046–2054 under RCP8.5 scenario. With daily averaged $PM_{2.5}$ surface concentration of 60 μg/m^3 defined as the threshold for such "unhealthy" extremes, high-PM extremes would occur 132 ± 8 days/year in the Decade 2050 under RCP8.5. Even more concerning, due to the potential health impacts of two stressors acting in tandem, is the joint occurrence of the heatwave and high-PM hazard (HHH), which would have substantial increases of 175% in frequency and 79% in duration. This is in contrast to the 73–76% increase for heatwave or high PM when assessed individually. The fraction of land exposed to prolonged HHH increases by more than tenfold in 2050. The alarming increases in just a few decades pose great challenges to adaptation and call for more aggressive mitigation. For example, under a lower emission pathway, the frequency of HHH will only increase by 58% with a lower frequency of high-PM extremes.

Plain Language Summary Extreme heat occurrence worldwide has increased in the past decades. At the same time, many cities are facing severe air pollution problems featuring high-PM episodes (high concentration of particulate matter due to various sources) that last from days to weeks. We present an integrated assessment of human exposure to the joint occurrence of the heatwave and high-PM extremes, and possible future changes have been missing. In addition to the expected elevation in the heatwave and high-PM-related extremes, we also show that the rare jointed events would have quite large increases in the future with a 175% increase in frequency. The fraction of land exposed to prolonged HHH would increase by more than tenfold in 2050. The alarming rate of increases in just a few decades pose great challenges to adaptation.

1. Introduction

South Asia is a home to more than 1.5 billion people and is under rapid economic growth with an expected population of 2 billion by the mid-21st century (Jones & O'Neill, 2016; Supporting Information Table S1). Among various environmental stresses, two prominent threats are heat extremes (Dash & Mamgain, 2011) and air quality degradation (Li et al., 2017), both of which are reported to lead to major public health crises (Azhar et al., 2014; Chowdhury et al., 2018).

Heat extremes adversely impact human health by affecting respiratory and cardiovascular systems and can also be associated with high surface ozone concentrations that have negative impacts on human health (e.g., Meehl et al., 2018). The heat hazard for human health is preferably quantified in

humidity-related temperature indices (Kovats & Hajat, 2008), such as wet-bulb temperature (Sherwood & Huber, 2010) or heat index (Anderson et al., 2013). These indices are related to the efficacy of releasing heat from the skin to regulate body temperature. Recent global climate model-based assessments show that the probability of reaching certain critical thresholds (jointly defined using temperature and relative humidity) empirically known to be life-threatening will continue to rise, especially over South Asia (e.g., Mora et al., 2017) because of the lower climate variability and the higher background humidity. The South Asia region is projected to experience more frequent heat extremes with longer duration and enhanced severity in the future (Russo et al., 2017), which is consistent with observed trends during the past few decades (Alexander, 2016; Dash & Mamgain, 2011; Basha et al., 2017; Pai et al., 2004; Khan et al., 2019; Yin & Sun, 2018).

While there have been major efforts to cut air pollution emissions in developing nations, South Asia faces a unique challenge because of ongoing industrialization and urbanization processes. The next few decades will witness a continued increase in air pollution emissions (or only slightly decrease) in certain Shared Socioeconomic Pathways (SSP)/Representative Concentration Pathway (RCP) scenarios (Rao et al., 2017), which is opposite to the projected worldwide reduction including East Asia. Thus, local emissions continue to be the primary driver for air quality issues, while the influence of climate change cannot be ignored as well (Xu & Lamarque, 2018; Wu et al., 2019).

Despite limited case studies on the urban heat island effect worsening air quality (Wilby, 2008) and potential positive feedback to further enhance heat stress (Cao et al., 2016) in megacities, a decade-long continental-scale analysis of the co-occurrence of heatwave and air pollution extremes and their future changes is still missing. Recent examples are analyses of the heatwave and ozone episodes, such as Schnell and Prather (2017) using North American observations and Meehl et al. (2018) using global model output.

Similarly, health risks associated with an elevated occurrence of heatwaves and high-PM weather are well studied, but often separately, highlighting a knowledge gap between understanding physical and chemical extremes. The compounding negative effect, when two types of conditions occur simultaneously, has only been studied at limited spatial scales (Doherty et al., 2009; Jackson et al., 2010; Stafoggia et al., 2008; Willers et al., 2016), including wildfire conditions induced by the 2010 Moscow heatwave. However, in the public health field, the synergistic impacts of two factors have raised great awareness on exacerbating health risks (De Sario et al., 2013; Katsouyanni & Analitis, 2009; Li et al., 2011; Nawrot et al., 2007; Qian et al., 2008; Ren et al., 2006).

2. Methods

2.1. Main Data Sets Used in This Study

This section briefly summarizes data sets used in this study, and detailed discussions are provided in the following sections.

1. WRF-Chem model simulation (Kumar et al., 2018) of 8 years for present-day (1997–2004) and 9 years for the mid-21st century (2046–2054) under RCP8.5 and RCP6.0 emission scenarios.
2. MERRA2 reanalysis products (Randles et al., 2017; Buchard et al., 2017) are used for surface $PM_{2.5}$, and ERA-Interim products (Dee et al., 2011) are used for deriving the wet-bulb temperature.
3. Ground measurement of daily temperature and relative humidity is from select airports (collected by the India Meteorological Department but downloaded free of charge from Weather Underground database).
4. Ground measurement of $PM_{2.5}$ in the late 1990s and early 2000s is compiled by Kumar et al. (2018), which is contributed by many observational studies (Balakrishnaiah et al., 2011; Deshmukh et al., 2013; Latha & Badarinath, 2003; Pillai et al., 2002; Tiwari et al., 2009; Tiwari et al., 2013).
5. Populations for present-day and future decades are based on Jones and O'Neill (2016). The spatially explicit population data set is from Jones and O'Neill with a spatial resolution of 1/8° by 1/8°. Before any data analysis related to population exposure, environmental quantities are regridded into the grid cells of population data using MATLAB function (interp2). SSP data are provided every 10 years between 2000 (base year) and 2100 (projections). For example, data are available for 2010, 2020, 2030, and so on. The Decade 2050 population projection (with 2 billion population in South Asia, Table S1) is based on Shared Socioeconomic Pathway (SSP) 5 scenario (fossil-fueled development for the economy), which

is consistent with RCP8.5 emission pathway. Other SSP scenarios compatible with other RCPs are available in Jones and O'Neill but are not used in this study.

2.2. Model

This study uses multiyear simulations conducted using a Nested Regional Climate model coupled with Chemistry (NRCM-Chem) that is based on the Weather Research and Forecasting (WRF) model coupled with Chemistry (WRF-Chem, Version 3.6.1) as described in Kumar et al. (2018). The model uses Model for Ozone and Related chemical Tracers, Version 4 (MOZART-4) (Emmons et al., 2010), for gas-phase chemistry and simulates major aerosol species including sulfate, nitrate, ammonium, organic carbon, black carbon, dust, and sea salt using the Model of Simulating Aerosol Interactions and Chemistry (Zaveri et al., 2008).

The model domain covers the entire South Asia and surrounding oceanic regions (1.5–44.7°N and 52.6–107.4°E) using two domains with coarser horizontal grid spacing (60 km) for the outer domain and finer horizontal grid spacing (12 km) for the smaller inner domain that encompasses the Indo-Gangetic Plain and the Himalayan region. All grid cells have the same area in this configuration. The simulation within the high-resolution inner domain only covers dry seasons (October to May) of each year. The model includes 51 vertical layers up to 10 hPa.

The Model of Simulating Aerosol Interactions and Chemistry includes a sophisticated aerosol thermodynamics module to simulate the effects of changes in temperature and humidity on gas-particle partitioning and on the intraparticle solid-liquid phase equilibrium. Meteorology and chemistry are fully coupled in NRCM-Chem and feedback to each other at every time step. Aerosols affect the meteorology by interacting with both the radiation and clouds, and the corresponding changes in meteorology (temperature, pressure, winds, solar radiation, planetary boundary layer height, and precipitation) affect trace gases and aerosols via feedback to atmospheric chemical kinetics, dry and wet deposition, transport, biogenic emissions, and boundary layer mixing. Fire emissions and land use types were kept constant between the present-day and future simulations to limit the number of drivers contributing to future changes in air quality.

2.3. Simulations

The historical simulation ("Decade 2000") is from 1997 to 2004, and the future simulation ("Decade 2050") is from 2046 to 2054. The simulation is driven by large-scale meteorological and chemical boundary conditions from a global climate model that has been bias corrected against past ERA-Interim (Bruyère et al., 2014). The evaluation of present-day climate and air quality also shows reasonable agreement (see evaluations in the supporting information), and identified meteorological bias was further corrected before our analysis (see supporting information for details). In a nutshell, we subtracted a geographically varying climatological bias as a function of time of the year (historical simulation against ERA-Interim) from both the historical and future simulations.

Due to high-resolution and complex chemical scheme, Kumar et al. (2018) only performed three sets of decade-long time-slice simulations, as opposed to a continuous century-long transient simulation such as in Xu and Lamarque (2018). Note that the decade-long time span of our simulation is still considerably longer than the most previous simulation with fine-resolution chemistry-climate models that usually lasted for weeks to months. The multiyear simulation with hourly output (averaged in this study to daily mean) of meteorology and chemistry is crucial to capture the behavior of extreme events (heatwave and high PM) and estimate future changes in their frequency.

2.4. Scenarios

The Decade 2000 simulation is driven by large-scale meteorological boundary conditions generated by Community Earth System Model Version 1 (CESM1; Hurrell et al., 2013), which is bias corrected towards the reanalysis data (European Reanalysis [ERA-Interim]) (Dee et al., 2011). The bias correction procedure is detailed in Bruyère et al. (2014). The chemical initial and boundary conditions are provided by a global atmospheric chemistry model (Community Atmospheric Model Version 4 with Chemistry, CAM4-Chem) (Lamarque et al., 2012), driven by the same meteorological fields from CESM1. Thus, the meteorological boundary conditions used for WRF-Chem are consistent with the chemical boundary conditions in these runs.

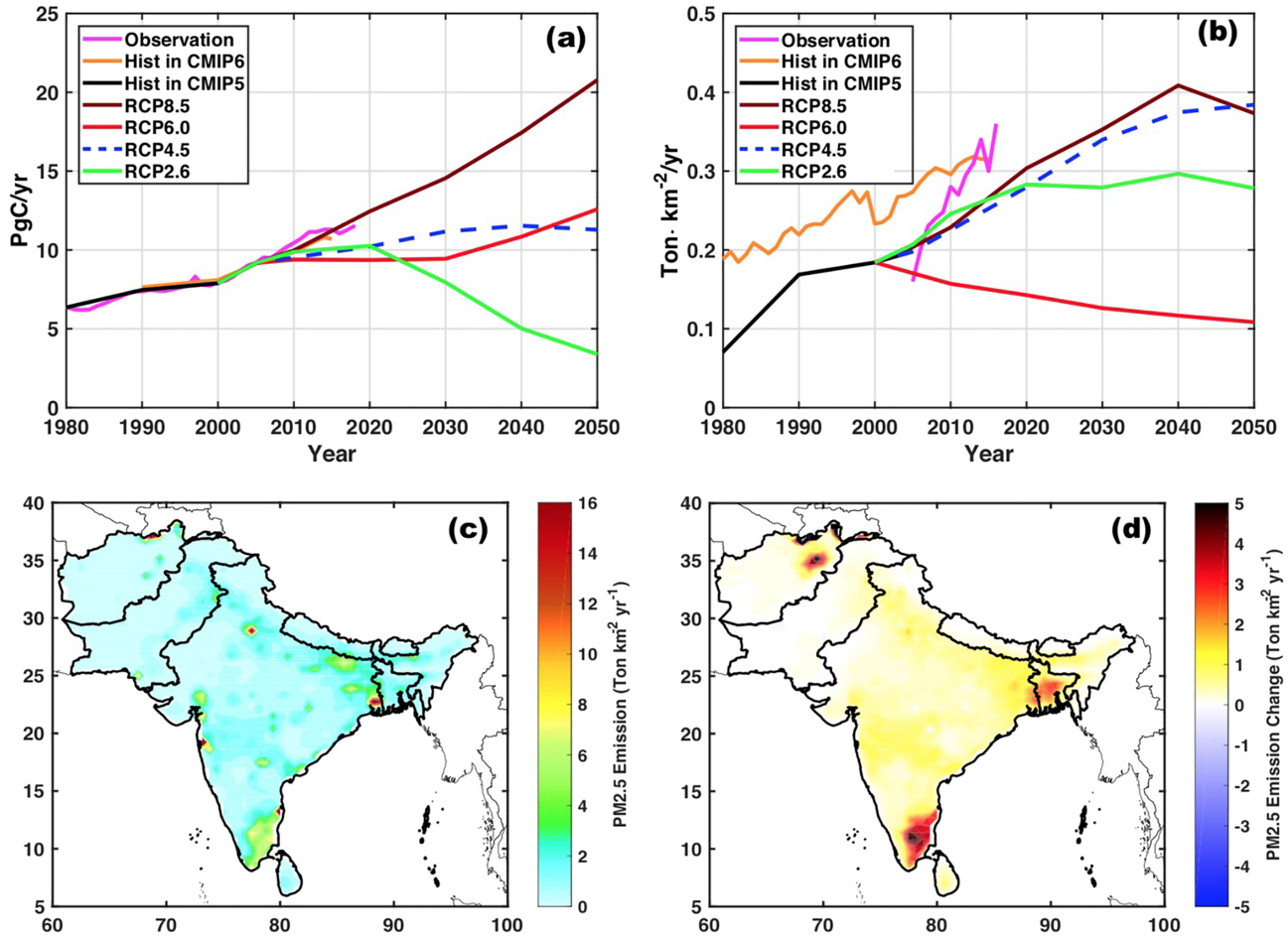

Figure 1. (a) Global emission of carbon (due to fossil fuel and land use) and (b) Indian emission of SO_2 under different projections. RCP4.5 curves are dashed to distinguish from the RCP8.5 curve in (b). The "history" is according to CMIP5 and CMIP6 protocol. Future emissions (after 2005) are from four RCP scenarios (van Vuuren et al., 2011). The CO_2 "observation" is from Le Quere et al. (2018). The Indian SO_2 "observation" is based on satellite estimates in Li et al. (2017). (c) Emission of $PM_{2.5}$ (ton km^{-2} $year^{-1}$) over South Asia in the Decade 2000 and (d) its change in the Decade 2050 under RCP8.5.

The emission data set was taken from the Atmospheric Chemistry and Climate Model Intercomparison Project (ACCMIP) (Lamarque et al., 2013). The simulated $PM_{2.5}$ surface concentration for the "Decade 2000" was evaluated against seven observational sites in South Asia, and five out of seven sites have a climatologically monthly mean bias of less than 10%. Note that in this paper we use "PM" as a broader term to refer those health-adverse fine particles ($PM_{2.5}$, particulate matter with a diameter less than 2.5 μm) while excluding the contribution of larger particles (>2.5 μm) that could also be important for surface visibility.

The Decade 2050 simulation is driven by CESM1 output under two future emission scenarios: RCP8.5 (CO_2 equivalent of 630 ppm in 2050) and RCP6.0 (505 ppm at 2050). The two scenarios considered are the two higher ones in the RCP database, and the global CO_2 emission is tracking RCP8.5 closely (as of 2018, Figure 1), justifying the focus on the two higher emission scenarios as opposed to the two lower ones. The $PM_{2.5}$ emission in South Asia stays largely the same under RCP6.0, compared to the historical period. But for RCP8.5, a 77% increase in total emission from the historical period level is projected. All four RCP scenarios could not be run because of limited computational and storage resources.

We note that the current global emission of CO_2 is tracking RCP8.5 closely (as of 2018, see Figure 1). The satellite-based SO_2 emission estimate (Li et al., 2017) is even higher than the RCP8.5 projection and more

in line with the recently released CMIP6 emission data set (SSP). These provide a strong justification for focusing on the higher emission scenario such as RCP8.5 as opposed to the lower ones.

2.5. Calculation of the Wet-Bulb Temperature (T_w)

Many previous heat extreme analyses only considered temperature alone (e.g., Meehl & Tebaldi, 2004; Xu et al., 2018), but more recent studies have accounted for humidity impact on the heat stress (e.g., Kovats & Hajat, 2008). A recent assessment of heat extremes related mortality suggested that a combination of temperature and humidity is a better metric to quantify health risks (Mora et al., 2017). That is, under high humidity conditions, human exposure to a lower temperature can induce the same level of risk compared to higher temperature exposure but under lower humidity conditions. Here, we account for both temperature and humidity variations by computing the wet-bulb temperature (T_w; Sherwood & Huber, 2010). T_w should not be confused with the wet-bulb globe temperature that additionally accounts for the effect of wind speed and solar radiation (or the simplified form by assuming moderate radiation and light wind speed as in Willett & Sherwood, 2012; Knutson & Ploshay, 2016).

In practice, wet-bulb temperature (T_w) can be measured by wet-bulb thermometers as the environment saturation ratio of water vapor is reached. Here T_w is computed following Stull (2011) from the daily average of T (temperature, "dry bulb"; unit: °C) and RH (relative humidity; unitless, ranging from 0% to 100%).

$$T_w = T\cdot\mathrm{atan}\left[0.151977(100\cdot\mathrm{RH}+8.313659)^{\frac{1}{2}}\right] + \mathrm{atan}(T+100\cdot\mathrm{RH}) - \mathrm{atan}(100\cdot\mathrm{RH}-1.676331) + 0.00391838(100\cdot\mathrm{RH})^{\frac{3}{2}}\mathrm{atan}(0.023101\cdot100\cdot\mathrm{RH}) - 4.686035$$

Depending on the data availability, RH is calculated in the following two ways.

1. From the WRF-Chem model output, RH is calculated from T (temperature; unit: K), p (air pressure; unit: Pa), and q (specific humidity; unitless).

$$e_s = e_0\exp\left(\frac{L_v}{R_w}\left(\frac{1}{T_0}-\frac{1}{T}\right)\right), \omega_s = \frac{R_a}{R_w}\frac{e_s}{p-e_s},\ \omega = \frac{q}{1-q},\ \mathrm{RH} = \frac{\omega}{\omega_s}100\%$$

2. From the ERA-Interim data set, RH is calculated from T, p, and T_{dew} (dew point temperature; unit: K).

$$e_s = e_0\exp\left(\frac{L_v}{R_w}\left(\frac{1}{T_0}-\frac{1}{T}\right)\right), e_{dew} = e_0\exp\left(\frac{L_v}{R_w}\left(\frac{1}{T_0}-\frac{1}{T_{dew}}\right)\right), \mathrm{RH} = \frac{e_{dew}}{e_s}\frac{p-e_s}{p-e_{dew}}100\%$$

In the equations above, e_0 (611 Pa) is the reference water vapor pressure, and e_s and e_{dew} are the water vapor pressure at saturation and at dew point temperature, respectively. w and w_s are water vapor mixing ratio (water vapor vs. dry air, unitless) at any given temperature or at saturation. T_0 (273 K) is the reference temperature. L_v (2.5×10^6 J/kg) is the latent heat of water vaporization (from liquid to gas). R_a (287 J/kg/K) is the specific gas constant for dry air. R_w (461.5 J/kg/K) is the specific gas constant for water vapor. Calculation of daily T_w has little differences from the mean-taking method, that is, from the average of hourly T_w or from mean daily T and RH (Figure S17).

2.6. Threshold for Defining Heatwave and High-PM Extremes

Here we adopt daily average T_w at 25 °C as the threshold for heat extremes in this analysis. This is close to the "deadly" threshold (red line in Figure 2) as reported in Mora et al. (2017) who established this threshold based on hundreds of heat-related deadly events during 1980 and 2014 and recorded daily temperature and humidity (but treated separately, not jointly using T_w).

In the context of weather extremes, the question often arises as to "how extreme" certain thresholds should be. Previous studies have used a higher threshold of 35 °C to identify deadly or even fatal extreme heat (Kang & Eltahir, 2018), which is the physical limit to heat removal from the body. Note that Lelieveld et al. (2014) used daily max temperature of 35 °C as the threshold, which is close to 25 °C T_w at 40% RH as in the two India heatwave events we identified (Figure 2), but not the wet-bulb temperature.

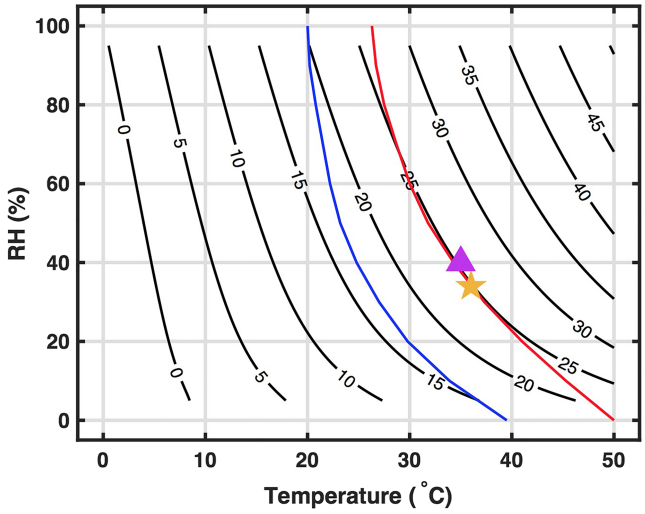

Figure 2. T_w as a function of temperature and relative humidity. The 25 °C T_w is close to the "deadly" threshold established in Mora et al. (2017) (red line, with 95% lethal events already occurring at this level). The blue line (T_w between 15 and 20 °C) is a weaker definition of heat extremes when the lethal events start to occur. Yellow star indicates a multiweek heat extremes event in Ahmedabad (in Western India) during May 2010 (T = 36 °C, RH = 34% from ERA-Interim monthly value; Azhar et al., 2014). The purple triangle indicates a heat extreme event in Allahabad (near central Indo-Gangetic Plain) during May 2015 (T = 35 °C, RH = 40% from ERA-Interim monthly value; Burke, 2015).

In our case, using the 25 °C threshold allows more samples to enter the analysis and provides a more robust statistical analysis. However, the results with a higher threshold (e.g., T_w of 28 °C, Table 1) would be qualitatively similar, the processes would be the same, and the basic results would not change with the caveat that the higher threshold would, of course, represent more lethal conditions. We also conducted a sensitivity test in Karachi using the threshold of daily maximum $T_w > 35$ °C (Table 1) following Kang and Eltahir (2018), which suggests that RCP8.5 could see a 720% increase in heat extreme frequency.

As acknowledged in Mora et al. (2017), previous assessments on deadly heat events have focused on developed nations in the Northern Hemisphere midlatitudes (Europe and North America). The applicability of the same threshold to tropical and developing nations remains to be tested using large-scale public health data. Here, we justify the robustness of the 25 °C T_w threshold with limited case studies over South Asia. The yellow star and purple triangle in Figure 2, both close to T_w of 25 °C, correspond to two heat extreme events, which reportedly killed more than 1,300 people (see Figure 2 caption for details).

It has become clear to the climate and health research community that the humidity effect needs to be accounted for in heat extreme health impact studies (Sherwood, 2018). To put T_w in the perspective of two other temperature/humidity-related heat metrics, T_w during the 2010 Ahmedabad event is 24.8 °C (T = 36 °C, RH = 34%), and this is equivalent to 37.2 °C in "heat index" (using the formula of http://www.wpc.ncep.noaa.gov/html/heatindex.shtml; Matthews et al., 2017, also called "apparent temperature"; Russo et al., 2017; Herring et al., 2016) and 41.6 °C (in "humidex" using the formula of https://memory.psych.mun.ca/tech/js/humidex) (Barnett et al., 2010). Such a high value of heat index is classified as "extreme caution" (https://www.weather.gov/safety/heat-index) by the National Oceanic and Atmospheric Administration, and such a high value of humidex is classified as "great discomfort" by the Canadian meteorologists (https://en.wikipedia.org/wiki/Humidex). Other more complex indices that use factors beyond the relative humidity may be more relevant to health impacts, such as wet-bulb globe temperature (Liang et al., 2011) or Universal Thermal Climate Index (Jendritzky et al., 2012).

Sustained exposure to high $PM_{2.5}$ environment (such as 100 μg/m^3) is conducive to cardiopulmonary mortality and lung cancer (Turner et al., 2011). The threshold of defining high-PM extremes days is here set to 60

Table 1
South Asia Frequency (Day/Year, the Map Shown in Figure S3) and Duration (Day, Map Is Shown in Figure S3) of Heat Extremes by Applying Different Thresholds

	Frequency (day/year)			Duration (day)		
Threshold definition	2000	2050 RCP6.0	2050 RCP8.5	2000	2050 RCP6.0	2050 RCP8.5
$T_w > 25$ °C	48	66	76	6	9	11
$T_w > 25$ °C but individual extreme event to be >2 days	38	54	65	7	12	18
$T_w > 18$ °C	168	183	191	75	119	141
$T_w > 28$ °C	2	5	10	1	1	2
$T > 31$ °C	49	56	63	8	9	10
$T_{w\_max} > 26$ °C	48	60	77	6	7	9
$T_{w\_max} > 35$ °C (as in Kang & Eltahir, 2018), for Karachi only	0.5	0.2	3.6	0.3	0.1	1.3

Note. All results are based on the original T_w (or T) without bias correction. The threshold of T (daily mean temperature) and T_{w_max} (daily maximum wet-bulb temperature) is deliberately selected so that the Decade 2000 frequency is similar to the frequency when using T_w of 25 °C as the threshold (48 days).

$\mu g/m^3$ of daily mean surface concentration of $PM_{2.5}$ following India air quality standard (CPCB, 2009). The 60-$\mu g/m^3$ value is larger than the "unhealthy" level of the 25 $\mu g/m^3$ recommended by the World Health Organization (2005) and the 55.5-$\mu g/m^3$ level of "unhealthy" recommended by the Environmental Protection Agency (2012) of the United States, but it is smaller than the 75-$\mu g/m^3$ definition of "severe air pollution" recommended in China (Jin et al., 2016). Sensitivity sensitivities (Figure S7) show the results are not particularly sensitive to the selection of threshold other than the expected absolute value change.

2.7. Statistical Metrics of Occurrence of Extreme Events (Heatwave and High PM)

To quantify the occurrence of the heatwave and high-PM extremes, the daily value of T_w and surface concentration of $PM_{2.5}$ are calculated for all grid points of the model output. Having established a certain threshold (section 4), days with values higher than the threshold are classified as extreme days. The frequency (days/year) and the mean duration (days) of extreme events are calculated for each year, and then, the multiyear average for the Decade 2000 and the Decade 2050 under RCP6.0/8.5 is taken to remove the interannual variability of regional climate. Using a stronger definition of extreme events that requires the duration of any individual events to be at least 2 days (e.g., Xu et al., 2018, and references within), the frequency numbers in Table S2 would be lower (see Table 1), but not significantly, due to the low weather variability and long-lasting nature of tropical heat extremes in this region.

In addition to quantities of the number of days of extremes, the severity of extremes is also important. The relative intensity of extreme events is reported here in an anomalous sense, as the difference between quantities averaged within extreme days and the selected threshold. A large relative intensity (°C or $\mu g/m^3$) indicates a severe departure from the threshold and has been suggested as a predictor for heat stress-related mortality (Rocklov et al., 2012).

We define a fourth metric here, accumulated relative intensity, as the product of frequency (days/year) and relative intensity (°C or $\mu g/m^3$). The concept of accumulated relative intensity for heat stress is similar to the cooling degree days ((temperature − 22 °C) * number of days with the temperature higher than 22 °C) that has been widely used in assessing the demand for air conditioning (Miller et al., 2008; Shi et al., 2016).

For detailed model setups, model evaluation, and wet-bulb temperature calculation, readers are referred to sections 2 to 4 of the supporting information.

3. Results

3.1. Humidity-Amplified Heat Stress

With the daily average wet-bulb temperature (T_w, as in Stull, 2011) of 25 °C as the threshold, heat extreme frequency is as high as 100–200 days/year over the coastal regions and the Indo-Gangetic Plains during the Decade 2000 (Figure S3), with a prolonged duration of more than 15 days particularly over the foothills of the Himalayas. The high values of T_w in the southern coastal regions are due to high humidity and in the Indo-Gangetic Plain due to high temperature (Figure S2). Under the RCP8.5 scenario, the future occurrence of heat extremes is projected to increase from 45 days/year (averaged over the seven countries within South Asia) to 78 days (a 73% increase; Table S2 and Figure 3) and with a mean duration of heat extreme events of over 14 days in cities such as Delhi (Table S5).

The intensification of heat extremes shown above is comparable to previous studies over this region when the uncertainty of regional warming projection is considered. In this study, there is projected regional warming of 1.6 °C from Decade 2000 to Decade 2050 (similar to Chaturvedi et al., 2012; 1.4 °C for T_w as in Table S2). More informative than the absolute value of change projected by a single model is how much of the enhancement, as shown above, can be mitigated by adopting a (moderately) low carbon emission pathway (e.g., RCP6.0). Our Decade 2050 simulation under RCP6.0 suggests that the increase in frequency and duration in RCP8.5 can be cut by 33% and 66%, respectively, over South Asia (Table S2). The relative magnitude is largely consistent with simulated lower regional warming (1.0 °C increase from now to midcentury in RCP6.0 compared to a 1.6 °C increase in RCP8.5), suggesting the scalability of heat extreme statistics shown here to other low-warming scenarios (e.g., RCP2.6), at least for this region. The fractional increase quantified in previous studies is somewhat different due to various definitions of heat extremes, which are discussed next.

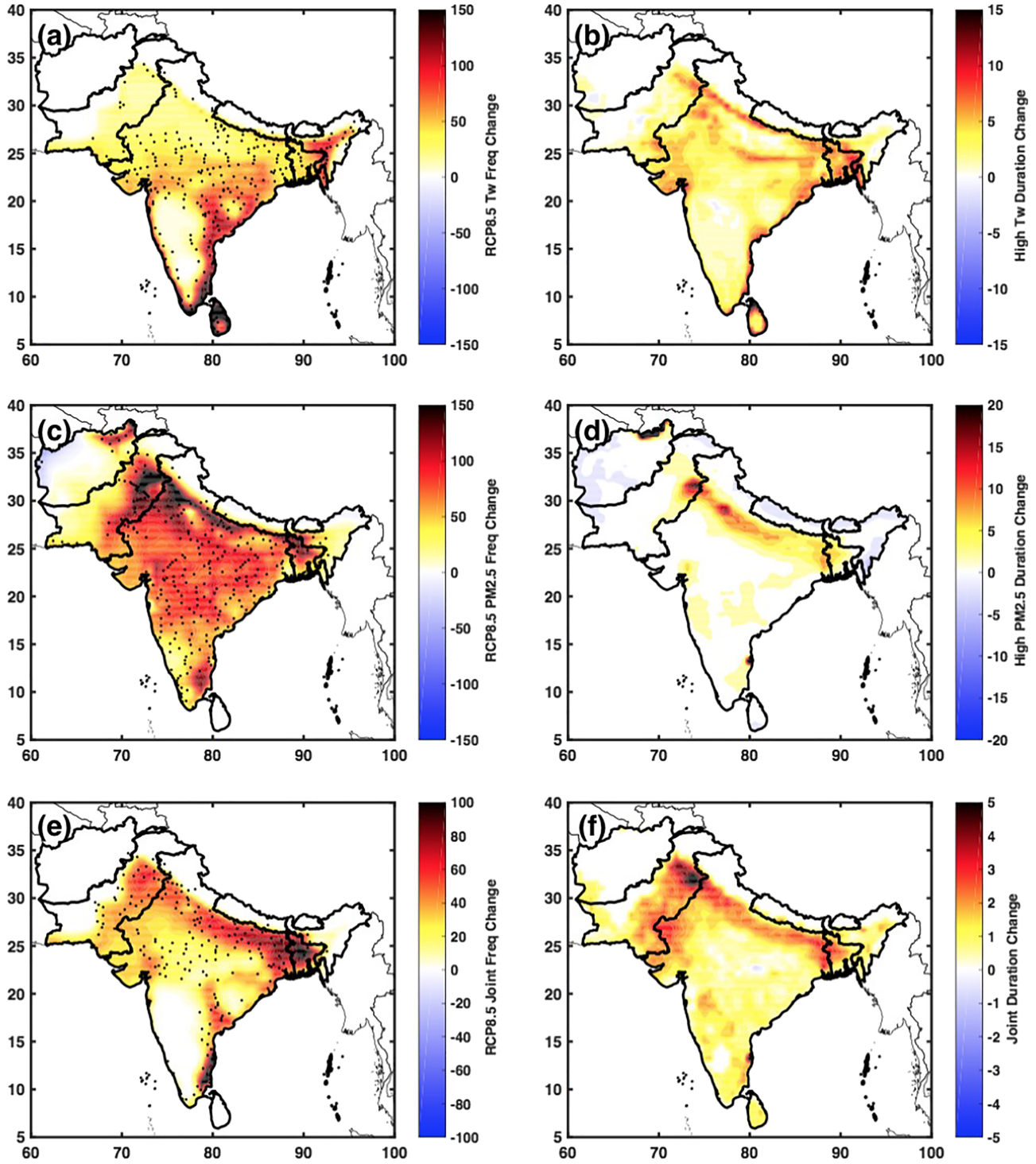

Figure 3. Future change (Decade 2050 minus Decade 2000) under RCP8.5 in frequency (days/year) of (a) heat extremes, (c) high-PM extremes, and (e) HHH. Stippling indicates regions with statistically significant positive change at the 1% confidence level using Student's *t* test. (b, d, and f) The same as the left column but for the mean duration (day).

The daily averaged T_w of 25 °C, at the 88th percentile of climatological T_w over South Asia (Table S2), may seem not very "extreme" but indeed corresponds to the level of heat stress experienced in two major multi-week heatwave episodes (May 2010 and May 2015) in India that reportedly led to thousands of deaths (Figure 2). As a sensitivity test, using a weaker threshold of 18 °C of T_w (the blue line in Figure 2, when

the heat-related causality just started to be reported as in Mora et al., 2017), the Decade 2000 occurrence is more frequent at 168 days/year, and the fractional increase into the future is much weaker (14%, Table 1) than when the 25 °C T_w is used as the threshold.

The lower thresholds of 18 and 25 °C T_w (following Mora et al., 2017) are established empirically based on numerous multidays to multiweek heatwave events that have led to major casualty to vulnerable groups such as children and elderly. The lower threshold of T_w should be clearly distinguished from T_w thresholds of 30 to 35 °C adopted in some earlier studies (Kang & Eltahir, 2018; Lemke & Kjellstrom, 2012; Sherwood & Huber, 2010; Van Oldenborgh et al., 2017; Table 1), which refers to a lethal physiologic limit that can cause instantaneous hyperthermia, even to healthy active outdoor workers, within just a few hours of exposure (presumably during the daytime).

When a higher threshold of T_w 28 °C is adopted as a sensitivity test, the Decade 2000 frequency is much rarer (2 days/year averaged across South Asia) compared to hundreds of days with heat stress when the lower thresholds of T_w were used, and the fractional increase in the future is, understandably, much stronger (>400%, Table 1). This is similar to the case when using a strict definition of heat extremes by requiring individual episodes to be at least two consecutive days (e.g., Xu et al., 2018). The relative future increase in frequency under this stricter requirement will also be larger (71% as opposed to 65%, Table 1).

Earlier studies, if using temperature alone without considering the humidity effect, omit the documented evidence that the human body responds negatively to high humidity conditions (Liu et al., 2014). Using temperature alone would underestimate the future increase of heat extremes. For example, if a threshold of $T > 31$ °C is selected (intentionally) that leads to a Decade 2000 frequency close to 48 days/year (similar to $T_w > 25$ °C, Table 1), the same model projects a 14–29% increase in frequency versus 38–58% using T_w and a 13–20% increase in duration versus 50–83% using T_w. The reason for the underestimation is that relative humidity over these tropical regions is projected by the latest global climate models to increase with global warming as well (Figures 6 and S2; see also Dai, 2006; Sherwood & Fu, 2014).

Even if the relative humidity stays the same, there will still be an underprediction of heat stress risks if using T alone, just because of the greater health effect of moisture in a warmer climate (Figure 2). The additional benefit of combining temperature and humidity in heat stress assessments is that the model deficiency in simulating the two (Figure S1; Willett & Sherwood, 2012) tends to offset. Similarly, the model discrepancies in projecting temperature and relative humidity tend to be the opposite (Fischer & Knutti, 2013).

A potential underestimation of future increase in heat stress is also likely in previous studies (e.g., Im et al., 2017) if using daily maximum temperature instead of daily mean temperature (unless the specific health and economic concern are lost labor hours and occupational mortality of outdoor workers). There is only a 25–60% increase in frequency when a T_{w_max} threshold of 26 °C is used (with the intention that a similar Decade 2000 frequency is found, Table 1), in contrast to the daily mean T_w used in this study (with a 38–58% increase in frequency). The future increase in health risk, when using T_{w_max} instead of daily averaged T_w as here, can be underestimated because (a) cooler nights can provide a relief period for the human body to rest and recover (Obradovich et al., 2017) and (b) nighttime temperatures tend to increase faster than daytime temperatures under global warming (Davy et al., 2017).

Are the simulations here (close to 10 years in each case) long enough to provide a robust projection of regional climate change? One may question that a single realization of 8 to 9 years might not be sufficient because a single decade of simulation can be heavily influenced by the phase of decadal variability mode such as AMO. We argue that our results are robust for the following two reasons: First, our simulation for Decade 2000 is highly constrained by observed meteorology (using ERA-Interim as the benchmark for bias correction) and thus represents the real meteorology as observed during those 8 years. Second, our Decade 2050 simulation is driven by boundary conditions provided by multiple runs from a global climate model (CESM1) and thus has effectively accounted for the decadal fluctuation of the climate system.

Are the projected changes here similar to other global climate models? The mean temperature for the South Asia region is 20.2 °C in the Decade 2000. At the Decade 2050, this region would experience a 1.5 °C warming compared to the Decade 2000 under RCP8.5 and a 1.0 °C warming under RCP6.0 (Figure S2, second row). These numbers are within the uncertainty range of global climate model output in Coupled Model Intercomparison Project Phase 5 (CMIP5), consistent with the fact that CESM1 has a moderate climate

Table 2
The Land Area Fraction Within South Asia That Is Exposed to 60 or More Days of Heat Extremes (Figure S3) and High-PM Extremes (Figure S5) and 60 More Days of Joint Events of Heatwave and High PM (Figure S6) and the Population Fraction

	Heat >60 days	High PM >60 days	Heatwave and high PM >60 days
Area fraction			
Decade 2000	35% (37%)	55%	2% (3%)
Decade 2050 under RCP6.0	48% (49%)	41%	10% (9%)
Decade 2050 under RCP8.5	56% (54%)	74%	25% (24%)
Population fraction			
Decade 2000	61% (64%)	73%	8% (9%)
Decade 2050 under RCP6.0	74% (74%)	62%	24% (21%)
Decade 2050 under RCP8.5	80% (80%)	90%	52% (50%)

Note. The numbers in parentheses are based on the original model output (without bias correction).

sensitivity compared with other CMIP5 models. For reference, the CMIP5 models yield a mean 2050 warming of 1.6 °C for RCP8.5 (Figure S2, fourth row) and 1.2 °C for RCP6.0 with an uncertainty of a few tenths of a degree (also seen in figure 6 of Chaturvedi et al., 2012).

3.2. Human Exposure to Elevated Heat Risks

Due to negative health consequences, it is important to assess human exposure to heat extremes and the reasons for future changes. In the top panels of Figure 4, we show the geographical distribution of population exposure to heat extreme frequency, which has higher values along the populated Indo-Gangetic Plain regions in Decade 2000. We find that population-weighted heat extreme frequency in the Decade 2000 is 83 days/year, larger than the area-weighted estimate (45 days/year), and is projected to increase by 51% to 125 days/year under RCP8.5 (Table S3). The population projection (under the SSP5 scenario; Jones & O'Neill, 2016) is spatially resolved and is consistent with the socioeconomic drivers of RCP emissions. Similar results were also found for the increase in heat extremes duration to 13 days (under RCP8.5) from 9 days in the Decade 2000 (Table S3).

The population-weighted average in Table S3 tends to be larger than the area-weighted results (Table S2) because populations are concentrated in the Indo-Gangetic Plain and coastal regions (Figure S4) where the heat extremes also tend to increase the most (Figure S3). The co-location of heat extremes and population density is particularly worrisome considering the lower income and GDP over the Indo-Gangetic Plain (Im et al., 2017), which suggests that the most vulnerable population groups will be subject to stronger heat extremes in the future.

Human exposure to heat extremes is dominated by three nations: Bangladesh, India, and Pakistan. Over India, 189.7 billion people-days of heat exposure per year are projected in the Decade 2050 (Table S4), a 149% increase from the Decade 2000. In the bottom panels of Figure 4, we also show another health-related quantity "accumulated relative intensity," which is the product of frequency (number of days) and relative intensity (T_w within extreme events minus the selected threshold) (Table S4 and Figure S5). This quantity factors in both the prolonged exposure and the severity of heat extremes. Decade 2050 will see 338 billion people °C days/year (under RCP8.5), a daunting 258% increase from the Decade 2000. The larger relative increase (258% vs. 149%) is consistent with the enhanced severity of heat extremes (with the relative intensity increasing from 1.0 to 1.7 °C) (Table S3 and Figure S3).

The increase in population exposure is due to three factors: future warming, population growth, and, to a lesser extent, population redistribution arising from migration and urbanization. The warming alone explains 41% of the total increase, while the population growth explains about 39% (Table S6). Interestingly, the redistribution of population in India (Figure S4c, while keeping total population fixed) also contributes 1.5% (1.6 billion people-day/year) of the total increase in human exposure to heat extremes (Table S6), which is due to future urbanization and well-captured urban heat island effects in this high-resolution regional climate model (Figure S3). We note that the exposure numbers presented here are the maximum potential human exposure (Mishra et al., 2017) that do not account for the time spent indoors with active cooling (which could also change from now to future due to air conditioning penetration into

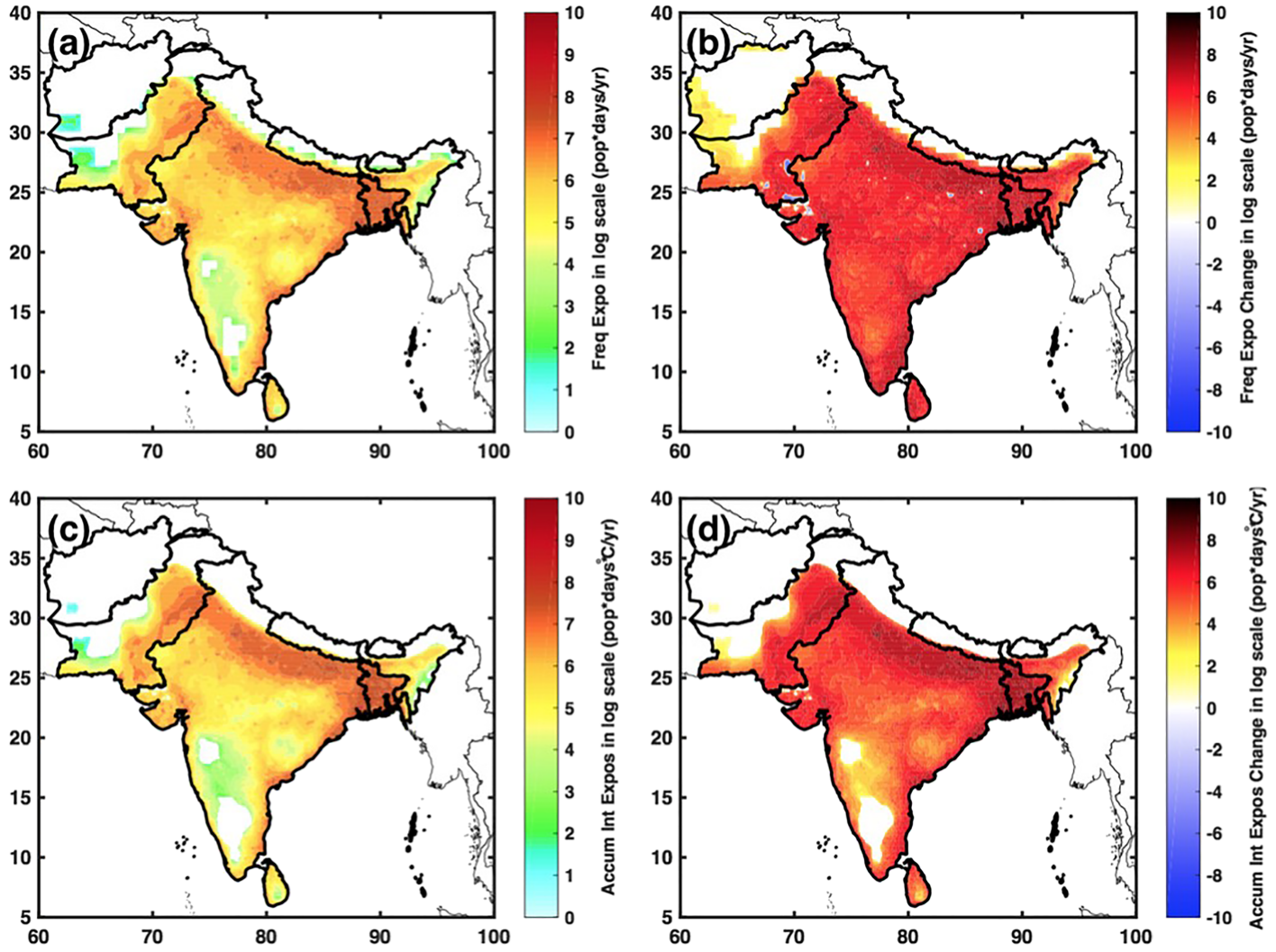

Figure 4. Population exposure to heat extreme frequency (population * frequency) in the (a) Decade 2000 and its change in the (b) Decade 2050 under RCP8.5. Note the logarithmic scale (1 for 10, 2 for 100, 3 for 1000, −1 for −10, −2 for −100, −3 for −1000, etc.). Population exposure to accumulated relative intensity (population * frequency * relative intensity) in the (c) Decade 2000 and its change in the (d) Decade 2050 under RCP8.5. The white areas within the thicker borderline are regions where no heat extremes occur in the Decade 2000.

household in developing countries; Auffhammer, 2014), which requires estimates of subdaily population distribution in cities.

In addition to the absolute value of human exposure, other important factors worth assessing are the fractions of population and land exposed to the prolonged heat extremes. In the Decade 2000, about 61% of the population within South Asia experienced heat extremes for more than 60 days per year, while in the future, 80% of the population will experience similar extreme heat conditions (Table 2). We estimate the total land fraction impacted by heat extremes for more than 60 days to be 35% in the Decade 2000 (Figure 7). That number will grow to 56% (RCP8.5) or 48% (RCP6.0) in the Decade 2050. Those estimates are robust regardless of whether the model simulated T_w is corrected based on reanalysis or not (Table 2).

3.3. A Hazier Future

Air pollution has been recognized as a modulating factor, which can affect the health impact of heat extremes (Gosling et al., 2009). Similar compounding effects have also been found when assessing air quality-related mortality as a function of background temperature (Jackson et al., 2010). We next describe the characteristics of high-PM extremes before discussing the joint occurrence and risk.

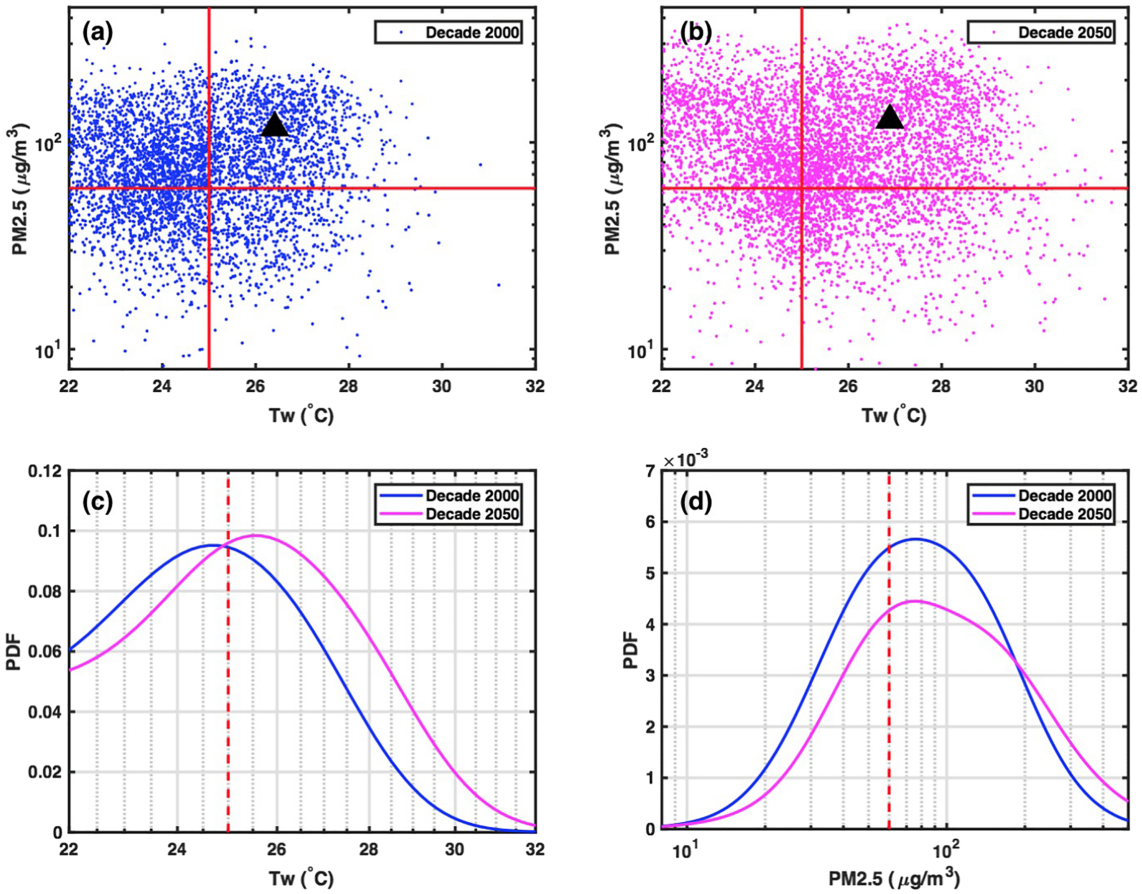

Figure 5. (a and b) The daily values over four major cities (Delhi, Mumbai, Dhaka, and Karachi). The *X*-axis is for T_w, and the *Y*-axis (in logarithmic scale) is for $PM_{2.5}$ surface concentration. (a) is for the Decade 2000, and (b) is for Decade 2050 under RCP8.5. Red horizontal and vertical lines are thresholds for heatwave and high-PM extremes. Black triangles indicate the average of all HHH events in the upper right quadrant. (c and d) Probability density function (PDF) for T_w and $PM_{2.5}$ over the four cities. Red dashed lines are thresholds for the heatwave and high-PM extremes.

When using daily average surface $PM_{2.5}$ mass concentration of 60 $\mu g/m^3$ as the definition of high-PM extremes (CPCB, 2009), we find an increase in the frequency and duration of high-PM extremes by 76% and 125%, respectively, from its Decade 2000 values of 75 ± 9 days/year (frequency) and 4 days (mean duration) (under RCP8.5; Table S2). This is in line with the mean $PM_{2.5}$ concentrations increase of 30% driven by an increase in regional PM emissions of 77% in RCP8.5 (Figure 1), while the climate change itself facilitates a stronger removal of $PM_{2.5}$ (Wu et al., 2019).

When using other threshold levels suggested by the World Health Organization, Environmental Protection Agency of the United States, or Chinese agencies, the main pattern of high-frequency regions remains the same, but the magnitude of future change would vary (Figure S7). If a lower threshold of air pollution is used, more days (actually most of the days in some cities) will be classified as "high-PM extremes," and its fractional increase into the future will be rather small. We here use a higher threshold of $PM_{2.5}$ to illustrate to the "extreme" nature of high-PM issues. Note that we also adopted a similar philosophy in choosing a higher threshold of heat (25 °C in T_w), again, to emphasize the rarity and extremity of those events.

Similar to heat extremes, population-weighted results are considerably higher than area-weighted results for the high-PM extremes. The population-weighted average of high-PM extremes frequency is 118 days/year (Table S3) compared to the area-weighted average of 75 days/year (Figure 7). This is a direct result of the strong co-location of emission sources (Figure 1), $PM_{2.5}$ concentrations (Figure S5), and the urban population (Figure S4).

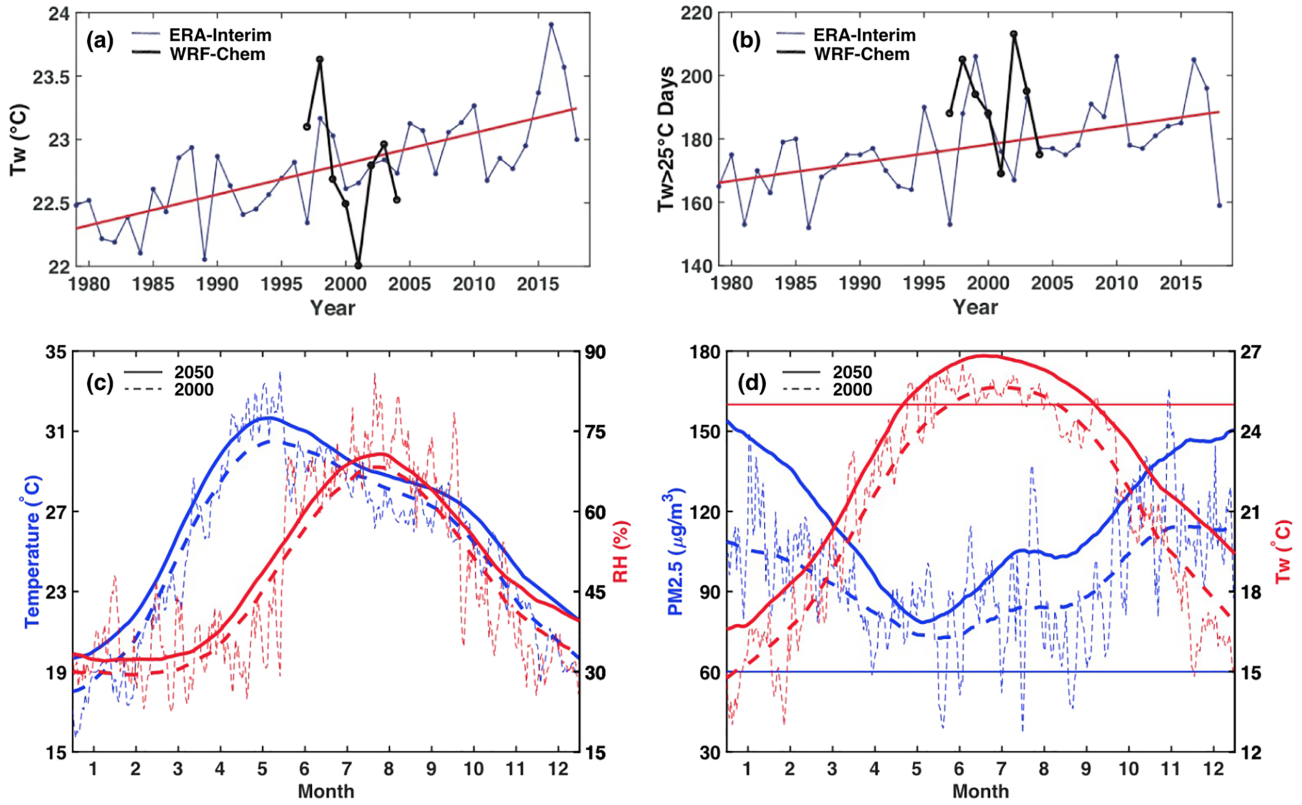

Figure 6. Simulated and observed changes over Dhaka, Bangladesh. (a) T_w in ERA-Interim (the thin blue line) and WRF-Chem (the thick black line). The red line is the linear fit of ERA-Interim data. (b) The same as (a) but for heat extreme frequency (day/year). (c) Climatologically averaged temperature based on WRF-Chem (blue, left *Y*-axis) and relative humidity (red, right *Y*-axis) as a function of the month. The thick dashed lines are for the Decade 2000, and the thick solid line is for the Decade 2050. The thin dashed lines with high-frequency fluctuation are the daily time series in the year of 1997. (d) The same as (c) but for WRF-Chem-simulated $PM_{2.5}$ and T_w (after the bias correction).

The population exposure to high-PM extremes frequency (number of people who experience extremes multiplied with the number of days exposed to the extreme; person * day/year) is projected to increase under RCP6.0 and RCP8.5 scenarios by 154% and 293% (Table S4), respectively. The lower population exposure to high-PM extremes under RCP6.0 is also largely due to lower emission growth. The population exposure to the accumulated relative intensity is 4.2 trillion people * $\mu g/m^3$ * day/year in the Decade 2000 and will increase by 293% in the Decade 2050. Note that the larger fractional change in accumulated relative intensity (as the product of frequency and relative intensity) indicates that the severity of high-PM extremes is getting worse (Figure S5). The multifold increase in human exposure is again driven by both population growth and worsening air quality. But in the case of high-PM extremes, the population growth plays a smaller role (19% due to population growth vs. 52% contributed by the hazier atmosphere). This is different from the stronger role of population growth for determining the increase in exposure to heat extremes (43% due to population growth vs. 38% due to warming). The urbanization effect is also more important for high PM (4.7% as opposed to 1.5% for heat shown previously, Table S6).

Since major air quality improvement initiatives have been planned by local governments, we also quantified the high-PM occurrences at the city level. Within South Asia, many cities are subject to a major increase in high-PM extremes but with different levels of severity (Table S5). For example, Mumbai is projected to experience a 34% increase in relative intensity. Cities such as Karachi are prone to the future growth of high-PM weather frequency by 37%, but some other cities appear to already experience ~300 days of high-PM extremes during the Decade 2000. The city-level results are not particularly sensitive to the spatial resolution of the model simulation. When the 12-km resolution simulation over the inner domain is utilized (higher than the 25 km used by Im et al., 2017, but lower than the 4-km grid resolution used by Hu et al., 2015, for the smaller California domain), both the present-day and future $PM_{2.5}$ in Delhi remain largely

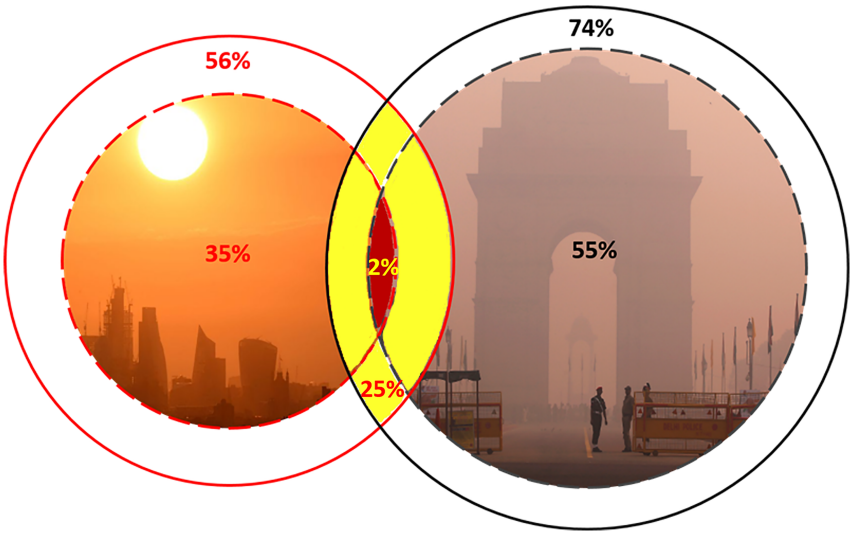

Figure 7. An illustration of the land fraction impacted by prolonged (60 days or more) extremes. The area of each circle corresponds to the South Asia land fraction with prolonged heat (red) and high-PM (black) extremes (Table 2). The smaller dash circles are Decade 2000, and the larger solid circles are Decade 2050. The overlapping area of smaller dash circles (red) and larger solid circles (yellow) corresponds to the multifold increase in the land area subjected to prolonged HHH (from 2% to 25%). The inserted images represent heat (left, credit: Toby Melville/REUTERS) and high-PM conditions (right, India Gate, credit: Adnan Abidi/REUTERS).

invariant compared to the 60-km simulation. However, the relative intensity for high-PM extremes documented here is slightly higher at 90.9 as opposed to 80.9 $\mu g/m^3$ (Table S5b).

3.4. Heatwave and High-PM Hazards

Lastly, we quantify the joint heatwave and high-PM hazards (HHH), which has been largely missing in all previous studies. The Decade 2000 frequency for HHH is low at 12 ± 2 days/year for South Asia (Figure 7) and 13 days/year for India (Table S7). In the Decade 2050, the frequency would increase to 33 ± 5 days/year, a 175% rise (under RCP8.5), much higher than the relative increase in heatwave or high PM alone (73% to 76%). A stronger enhancement in HHH is also seen for other extreme quantities such as the mean duration (with a relative increase of 79%) and the relative intensity (with an increase of 0.4 °C and 7.0 $\mu g/m^3$) (Figures 8 and S6).

The changes in HHH are driven mostly by a larger increase over the spring to summer transitional period, and that results in a greater number of days falling into the high-T_w/high-PM quadrant as illustrated in Figure 5 using the data over the four cities. Figure 6 (bottom panels) shows the seasonal variation of temperature, RH, T_w, and $PM_{2.5}$. Moist monsoon season is cooler than the pre-monsoon season, but accounting for the humidity effects leads to an extended "hot" season (see T_w during April to October in Figure 6). A key feature is the extension of pre-monsoon high PM (pollution season) into the monsoonal season and, concurrently, the extension of heat extremes into pre-monsoon season. These two factors, when simultaneously occurring, contribute to the multifold increase in the frequency of the joint hazards.

The rarity of HHH frequency in the Decade 2000 also means there is a larger relative change in the future for area and population impacted by prolonged HHH events (a factor of 12 increase for exposed land area and a factor of 6.5 increase for the exposed population; Table S2). The multifold increase in the land or population fraction affected by HHH, as opposed to the 31–60% increase in heat-affected and 23–35% high-PM-affected land or population fraction, when computed separately, is the most remarkable message of this study (Table S2 and Figure 7). The multifold increase in land exposed to HHH is illustrated in Figure 7 by the overlapping area of black and red circles and will pose significant difficulties for adaptation. Given the potential underestimation of HHH health impacts, our results suggest that a major increase in HHH-related mortality is on the horizon. Evidence-based quantification of HHH-related mortality is clearly needed to account for the compounding effects of two types of extremes and also to avoid double counting when linearly adding the mortality estimates from empirical approaches.

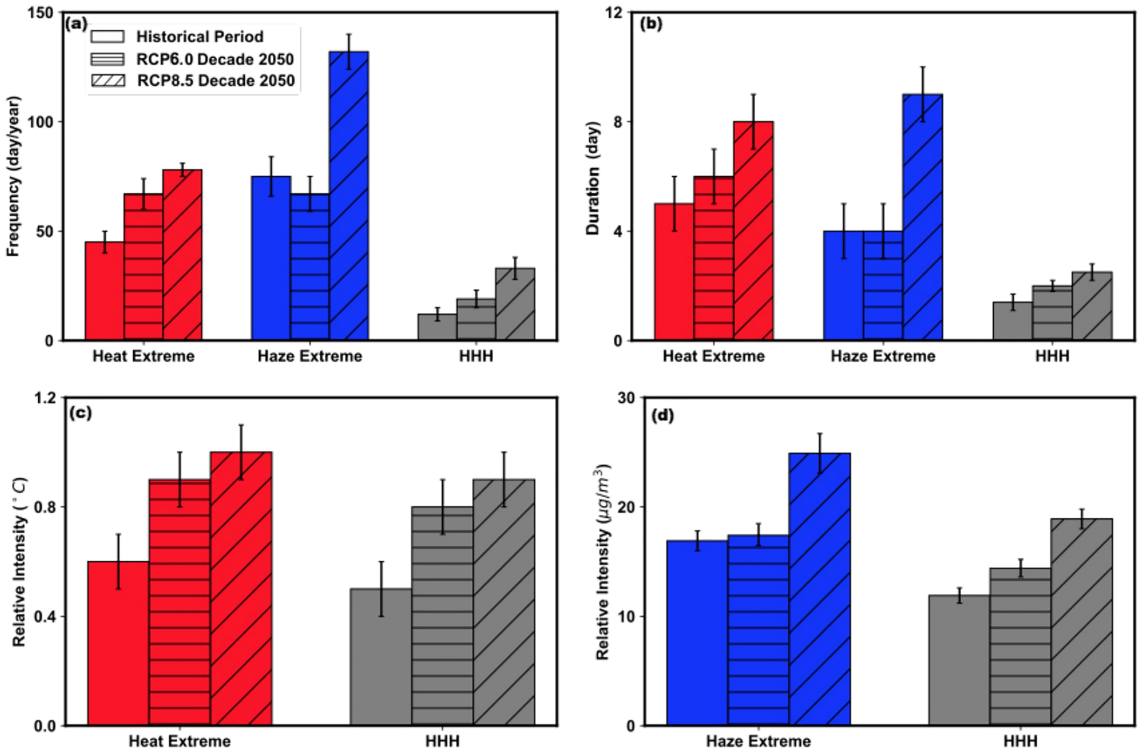

Figure 8. (a) frequency, (b) duration of heat extremes (red), high-PM extremes (blue), and HHH (gray). (c) The relative intensity of heat extremes and HHH in °C. (d) The relative intensity of high-PM extremes and HHH in $\mu g/m^3$. All data are for South Asia (Decade 2000 and Decade 2050 under RCP6.0 and RCP8.5). Error bars are the standard deviation showing inter-annual variability. More statistics can be found in Table S2 and Figure S9.

Although beyond the scope of the paper, one can investigate extreme ozone (e.g., >70 ppb) because many of these regions are very prone to temperature-ozone overlap. Therefore, it will be interesting to assess the occurrence of all three. Our model simulates ozone concentration well (Kumar et al., 2018), even though one limitation of the current WRF-Chem simulations is that it does not include ozone-radiation interactions, which might be not as large as aerosol effects.

However, in general, the monthly mean value rarely exceeds 70 ppb (see Dhaka in figure 4 of Kumar et al., 2018); thus, ozone is less of concern for local air quality as of now. Note that it is possible the NO_x to volatile organic compound ratios will change and ozone will be in exceedance in the future, which has started to happen in China. For North America and other regions, the co-occurrence of heat extreme and ozone can also be very important, as recently studied by Schnell and Prather (2017) and Meehl et al. (2018). Thus, the extreme occurrence of all three could be a very interesting question to look at in future studies, for other regions.

4. Concluding Remarks

Heat extreme occurrence worldwide has increased in the past decades, especially when accounting for the amplification due to the humidity effect and urban heat island influences. At the same time, many cities are facing severe air pollution problems featuring high-PM episodes (high concentration of particulate matter due to various sources) that last from days to weeks. Despite the potential compounding effects on vulnerable population groups and complex dynamical-physical-chemical interactions, the characteristics and potential predictive skills of the co-occurrence of HHH have not been extensively studied.

Although previous studies have suggested common meteorological drivers for these two types of extremes (Schnell & Prather, 2017) and potential amplifying feedbacks (Cao et al., 2016), an integrated assessment of human exposure to the joint occurrence of heatwave and high-PM extremes and possible future changes has been missing (except for a few studies at local scale; Doherty et al., 2009; Jackson et al., 2010).

A regional-scale assessment for the present-day heatwave and high-PM occurrence and future changes is presented here. The most crucial result here is that the frequency of these rare HHH events would

increase by 175% in the future, which is in contrast to the 73–76% increase when heatwave or high PM is assessed individually. Consequently, the land fraction affected by prolonged exposure to HHH events will increase by more than tenfold rather than 35% to 60% when the heatwave or high PM are studied separately. The unprecedented worsening of air quality and regional climate, if occurring in just a few decades, poses great challenges to adaptation. If the air pollution emission were not elevated as much as in projected in RCP8.5, then the high-PM extreme will not worsen. For example, under RCP6.0, the frequency of high PM will decrease by 11%, and HHH will only increase by 58%.

Our results suggest that the thermodynamic effect of regional warming leads to the increase in heat extremes and the PM emission increase (as assumed in RCP8.5) is the first-order factor leading to an increase in the high-PM extremes. Other questions remain. How would atmospheric circulation (stagnation) and precipitation play a secondary role? How do the high PM and heat interact with each other (e.g., heat extreme amplifying the high-PM concentration or a high-PM layer mitigating the intensity of urban heat island which seems to be suggested by Figures 8c)? Those will need to be addressed in future studies because of the limitation of the current model setup. The main purpose of this study is to bring forth a greater awareness of the potential larger increase in the coincidence of two stressors. Our results have broad implications, both scientifically and societally. The quantification, projection, and communication of joint risks of the co-occurrence of physical and chemical weather extremes are important for public health and urban planning. The mechanisms have been examined before for individual cases, but the findings are often scattered among different research communities with limited integration. A holistic view of the health impacts of the HHH is therefore urgently needed.

Data Availability Statement

The WRF-Chem simulation data are stored on NCAR High Performance Storage System (HPSS) under the following directory: /home/rkumar and are also publicly available at Research Data Archive https://rda.ucar.edu/. The observational and reanalysis data set is publicly available at their original sources as detailed in section 2.

Acknowledgments
We thank three anonymous reviewers for comments. We appreciate useful discussions with Claudia Tebaldi. Y. X. thanks partial support from Texas A&M University School of Innovation (Innovation[X] program) and the National Science Foundation (AGS-1841308). X. W. thanks NCAR Advanced Study Program (ASP) graduate visitor program. L. L. is supported by the key National Natural Science Foundation of China (91644225). We would like to acknowledge high-performance computing support from Yellowstone (ark:/85065/d7wd3xhc) provided by NCAR's Computational and Information Systems Laboratory, sponsored by the National Science Foundation. Portions of this study were supported by the Regional and Global Model Analysis (RGMA) component of the Earth and Environmental System Modeling Program of the U.S. Department of Energy's Office of Biological & Environmental Research (BER) via National Science Foundation IA 1844590. This work also was supported partially by the National Center for Atmospheric Research, which is a major facility sponsored by the National Science Foundation under Cooperative Agreement No. 1852977.

References

Alexander, L. V. (2016). Global observed long-term changes in temperature and precipitation extremes: A review of progress and limitations in IPCC assessments and beyond. *Weather and Climate Extremes*, *11*, 4–16.

Anderson, G. B., Bell, M. L., & Peng, R. D. (2013). Methods to calculate the heat index as an exposure metric in environmental health research. *Environmental Health Perspectives*, *121*(10), 1111–1119. https://doi.org/10.1289/ehp.1206273

Auffhammer, M. (2014). Cooling China: The weather dependence of air conditioner adoption. *Frontiers of Economics in China*, *9*(1), 70–84.

Azhar, G. S., Mavalankar, D., Nori-Sarma, A., Rajiva, A., Dutta, P., Jaiswal, A., et al. (2014). Heat-related mortality in India: Excess all-cause mortality associated with the 2010 Ahmedabad heat wave. *PLoS ONE*, *9*(3), e91831. https://doi.org/10.1371/journal.pone.0091831

Barnett, A. G., Tong, S., & Clements, A. C. (2010). What measure of temperature is the best predictor of mortality? *Environmental Research*, *110*(6), 604–611.

Balakrishnaiah, G., Kumar, K. R., Reddy, B., Gopal, K. R., Reddy, R. R., Reddy, L. S. S., et al. (2011). Characterization of PM, PM_{10} and $PM_{2.5}$ mass concentrations at a tropical semi-arid station in Anantapur, India. 92.60. Mt; 92.60. Sz.

Basha, G., Kishore, P., Ratnam, M. V., Jayaraman, A., Kouchak, A. A., Ouarda, T. B., & Velicogna, I. (2017). Historical and Projected Surface Temperature over India during the 20th and 21st century. *Scientific Reports*, *7*(1), 2987.

Bruyère, C. L., Done, J. M., Holland, G. J., & Fredrick, S. (2014). Bias corrections of global models for regional climate simulations of high-impact weather. *Climate Dynamics*, *43*(7-8), 1847–1856. https://doi.org/10.1007/s00382-013-2011-6

Buchard, V., Randles, C. A., Da Silva, A. M., Darmenov, A., Colarco, P. R., Govindaraju, R., et al. (2017). The MERRA-2 aerosol reanalysis, 1980 onward. Part II: Evaluation and case studies. *Journal of Climate*, *30*(17), 6851–6872.

Burke, J. (2015). India heatwave kills more than 500 people. https://www.theguardian.com/world/2015/may/25/india-heatwave-deaths-heatstroke-temperatures

Cao, C., Lee, X., Liu, S., Schultz, N., Xiao, W., Zhang, M., & Zhao, L. (2016). Urban heat islands in China enhanced by high-PM pollution. *Nature Communications*, *7*, 12509.

Chaturvedi, R. K., Joshi, J., Jayaraman, M., Bala, G., & Ravindranath, N. H. (2012). Multi-model climate change projections for India under representative concentration pathways. *Current Science*, 791–802.

Chowdhury, S., Dey, S., & Smith, K. R. (2018). Ambient $PM_{2.5}$ exposure and expected premature mortality to 2100 in India under climate change scenarios. *Nature Communications*, *9*(1), 318.

CPCB (2009). National Ambient Air Quality Status 2009. http://cpcb.nic.in/cpcbold/upload/Publications/Publication_514_airqualitystatus2009.pdf

Dai, A. (2006). Recent climatology, variability, and trends in global surface humidity. *Journal of Climate*, *19*(15), 3589–3606.

Dash, S. K., & Mamgain, A. (2011). Changes in the frequency of different categories of temperature extremes in India. *Journal of Applied Meteorology and Climatology*, *50*(9), 1842–1858.

Davy, R., Esau, I., Chernokulsky, A., Outten, S., & Zilitinkevich, S. (2017). Diurnal asymmetry to the observed global warming. *International Journal of Climatology*, *37*(1), 79–93.

De Sario, M., Katsouyanni, K., & Michelozzi, P. (2013). Climate change, extreme weather events, air pollution and respiratory health in Europe. *European Respiratory Journal*, *42*(3), 826–843.

Dee, D. P., Uppala, S. M., Simmons, A. J., Berrisford, P., Poli, P., Kobayashi, S., et al. (2011). The ERA-Interim reanalysis: Configuration and performance of the data assimilation system. *Quarterly Journal of the Royal Meteorological Society*, *137*(656), 553–597. https://doi.org/10.1002/qj.828

Deshmukh, D. K., Deb, M. K., & Mkoma, S. L. (2013). Size distribution and seasonal variation of size-segregated particulate matter in the ambient air of Raipur City, India. *Air Quality, Atmosphere and Health*, *6*(1), 259–276.

Doherty, R. M., Heal, M. R., Wilkinson, P., Pattenden, S., Vieno, M., Armstrong, B., et al. (2009). Current and future climate- and air pollution-mediated impacts on human health. *Environmental Health*, *8*, S8. https://doi.org/10.1186/1476-069X-8-S1-S8

Emmons, L. K., Walters, S., Hess, P. G., Lamarque, J. F., Pfister, G. G., Fillmore, D., et al. (2010). Description and evaluation of the Model for Ozone and Related chemical Tracers, Version 4 (MOZART-4). *Geoscientific Model Development*, *3*, 43–67.

EPA (2012). https://www.epa.gov/sites/production/files/2016-04/documents/2012_aqi_factsheet.pdf

Fischer, E. M., & Knutti, R. (2013). Robust projections of combined humidity and temperature extremes. *Nature Climate Change*, *3*(2), 126–130.

Gosling, S. N., McGregor, G. R., & Lowe, J. A. (2009). Climate change and heat-related mortality in six cities part 2: Climate model evaluation and projected impacts from changes in the mean and variability of temperature with climate change. *International Journal of Biometeorology*, *53*(1), 31–51. https://doi.org/10.1007/s00484-008-0189-9

Herring, S. C., Hoell, A., Hoerling, M. P., Kossin, J. P., Schreck, C. J. III, & Stott, P. A. (2016). Explaining extreme events of 2015 from a climate perspective. *Bulletin of the American Meteorological Society*, *97*(12), S1–S145.

Hu, J., Zhang, H., Ying, Q., Chen, S. H., Vandenberghe, F., & Kleeman, M. J. (2015). Long-term particulate matter modeling for health effect studies in California—Part 1: Model performance on temporal and spatial variations. *Atmospheric Chemistry and Physics*, *15*(6), 3445–3461.

Hurrell, J. W., Holland, M. M., Gent, P. R., Ghan, S., Kay, J. E., Kushner, P. J., et al. (2013). The community earth system model: A framework for collaborative research. *Bulletin of the American Meteorological Society*, *94*(9), 1339–1360.

Im, E. S., Pal, J. S., & Eltahir, E. A. (2017). Deadly heat waves projected in the densely populated agricultural regions of South Asia. *Science Advances*, *3*(8), e1603322. https://doi.org/10.1126/sciadv.1603322

Jackson, J. E., Yost, M. G., Karr, C., Fitzpatrick, C., Lamb, B. K., Chung, S. H., et al. (2010). Public health impacts of climate change in Washington State: Projected mortality risks due to heat events and air pollution. *Climatic Change*, *102*(1-2), 159–186.

Jendritzky, G., de Dear, R., & Havenith, G. (2012). UTCI—Why another thermal index? *International Journal of Biometeorology*, *56*(3), 421–428. https://doi.org/10.1007/s00484-011-0513-7

Jin, Y., Andersson, H., & Zhang, S. (2016). Air pollution control policies in China: A retrospective and prospects. *International Journal of Environmental Research and Public Health*, *13*(12), 1219.

Jones, B., & O'Neill, B. C. (2016). Spatially explicit global population scenarios consistent with the Shared Socioeconomic Pathways. *Environmental Research Letters*, *11*(8), 084003.

Kang, S., & Eltahir, E. A. (2018). North China Plain threatened by deadly heatwaves due to climate change and irrigation. *Nature Communications*, *9*(1), 2894. https://doi.org/10.1038/s41467-018-05252-y

Katsouyanni, K., & Analitis, A. (2009). Investigating the synergistic effects between meteorological variables and air pollutants: Results from the European PHEWE, EUROheatwave and CIRCE projects. *Epidemiology*, *20*(6), S264.

Khan, N., Shahid, S., Bin Ismail, T., & Wang, X. J. (2019). Spatial distribution of unidirectional trends in temperature and temperature extremes in Pakistan. *Theoretical and Applied Climatology*, *136*(3-4), 899–913.

Knutson, T. R., & Ploshay, J. J. (2016). Detection of anthropogenic influence on a summertime heat stress index. *Climatic Change*, *138*(1-2), 25–39.

Kovats, R. S., & Hajat, S. (2008). Heat stress and public health: A critical review. *Annual Review of Public Health*, *29*(1), 41–55. https://doi.org/10.1146/annurev.publhealth.29.020907.090843

Kumar, R., Barth, M. C., Pfister, G. G., Delle Monache, L., Lamarque, J. F., Archer-Nicholls, S., et al. (2018). How will air quality change in South Asia by 2050? *Journal of Geophysical Research: Atmospheres*, *123*, 1840–1864. https://doi.org/10.1002/2017JD027357

Lamarque, J. F., Emmons, L. K., Hess, P. G., Kinnison, D. E., Tilmes, S., Vitt, F., et al. (2012). CAM-chem: Description and evaluation of interactive atmospheric chemistry in the Community Earth System Model. *Geoscientific Model Development*, *5*(2), 369.

Lamarque, J. F., Shindell, D. T., Josse, B., Young, P., Cionni, I., Eyring, V., et al. (2013). The Atmospheric Chemistry and Climate Model Intercomparison Project (ACCMIP): Overview and description of models, simulations and climate diagnostics. *Geoscientific Model Development*, *6*(1), 179–206.

Latha, K. M., & Badarinath, K. V. S. (2003). Black carbon aerosols over tropical urban environment—A case study. *Atmospheric Research*, *69*(1-2), 125-133.

Lelieveld, J., Hadjinicolaou, P., Kostopoulou, E., Giannakopoulos, C., Pozzer, A., Tanarhte, M., & Tyrlis, E. (2014). Model projected heat extremes and air pollution in the eastern Mediterranean and Middle East in the twenty-first century. *Regional Environmental Change*, *14*(5), 1937–1949.

Le Quéré, C., Andrew, R. M., Friedlingstein, P., Sitch, S., Hauck, J., Pongratz, J., et al. (2018). Global carbon budget 2018. *Earth System Science Data (Online)*, *10*(4), 2141–2194. https://doi.org/10.5194/essd-10-2141-2018

Lemke, B., & Kjellstrom, T. (2012). Calculating workplace WBGT from meteorological data: A tool for climate change assessment. *Industrial Health*, *50*(4), 267–278. https://doi.org/10.2486/indhealth.ms1352

Li, C., McLinden, C., Fioletov, V., Krotkov, N., Carn, S., Joiner, J., et al. (2017). India is overtaking China as the world's largest emitter of anthropogenic sulfur dioxide. *Scientific Reports*, *7*(1), 14304. https://doi.org/10.1038/s41598-017-14639-8

Li, G., Zhou, M., Cai, Y., Zhang, Y., & Pan, X. (2011). Does temperature enhance acute mortality effects of ambient particle pollution in Tianjin City, China. *Science of the Total Environment*, *409*(10), 1811–1817. https://doi.org/10.1016/j.scitotenv.2011.02.005

Liang, C., Zheng, G., Zhu, N., Tian, Z., Lu, S., & Chen, Y. (2011). A new environmental heat stress index for indoor hot and humid environments based on Cox regression. *Building and Environment*, *46*(12), 2472–2479.

Liu, H., Liao, J., Yang, D., Du, X., Hu, P., Yang, Y., & Li, B. (2014). The response of human thermal perception and skin temperature to step-change transient thermal environments. *Building and Environment*, *73*, 232–238.

Matthews, T. K., Wilby, R. L., & Murphy, C. (2017). Communicating the deadly consequences of global warming for human heat stress. *Proceedings of the National Academy of Sciences*, 201617526.

Meehl, G. A., & Tebaldi, C. (2004). More intense, more frequent, and longer lasting heat waves in the 21st century. *Science*, *305*(5686), 994–997. https://doi.org/10.1126/science.1098704

Meehl, G. A., Tebaldi, C., Tilmes, S., Lamarque, J. F., Bates, S., Pendergrass, A., & Lombardozzi, D. (2018). Future heat waves and surface ozone. *Environmental Research Letters*, *13*(6), 064004.

Miller, N. L., Hayhoe, K., Jin, J., & Auffhammer, M. (2008). Climate, extreme heat, and electricity demand in California. *Journal of Applied Meteorology and Climatology*, *47*(6), 1834–1844.

Mishra, V., Mukherjee, S., Kumar, R., & Stone, D. A. (2017). Heat wave exposure in India in current, 1.5 C, and 2.0 C worlds. *Environmental Research Letters*, *12*(12), 124012.

Mora, C., Dousset, B., Caldwell, I. R., Powell, F. E., Geronimo, R. C., Bielecki, C. R., et al. (2017). Global risk of deadly heat. *Nature Climate Change*, *7*(7), 501.

Nawrot, T. S., Torfs, R., Fierens, F., De Henauw, S., Hoet, P. H., Van Kersschaever, G., et al. (2007). Stronger associations between daily mortality and fine particulate air pollution in summer than in winter: Evidence from a heavily polluted region in western Europe. *Journal of Epidemiology & Community Health*, *61*(2), 146–149. https://doi.org/10.1136/jech.2005.044263

Obradovich, N., Migliorini, R., Mednick, S. C., & Fowler, J. H. (2017). Nighttime temperature and human sleep loss in a changing climate. *Science Advances*, *3*(5), e1601555. https://doi.org/10.1126/sciadv.1601555

Pai, D. S., Thapliyal, V., & Kokate, P. D. (2004). Decadal variation in the heatwave and cold waves over India during 1971–2000. *Mausam*, *55*(2), 281–292.

Pillai, P. S., Babu, S. S., & Moorthy, K. K. (2002). A study of PM, PM_{10} and $PM_{2.5}$ concentration at a tropical coastal station. *Atmospheric Research*, *61*(2), 149–167.

Qian, Z., He, Q., Lin, H. M., Kong, L., Bentley, C. M., Liu, W., & Zhou, D. (2008). High temperatures enhanced acute mortality effects of ambient particle pollution in the "oven" city of Wuhan, China. *Environmental Health Perspectives*, *116*(9), 1172–1178. https://doi.org/10.1289/ehp.10847

Randles, C. A., Da Silva, A. M., Buchard, V., Colarco, P. R., Darmenov, A., Govindaraju, R., et al. (2017). The MERRA-2 aerosol reanalysis, 1980 onward. Part I: System description and data assimilation evaluation. *Journal of Climate*, *30*(17), 6823–6850.

Rao, S., Klimont, Z., Smith, S. J., Van Dingenen, R., Dentener, F., Bouwman, L., et al. (2017). Future air pollution in the Shared Socio-economic Pathways. *Global Environmental Change*, *42*, 346–358.

Ren, C., Williams, G. M., & Tong, S. (2006). Does particulate matter modify the association between temperature and cardiorespiratory diseases? *Environmental Health Perspectives*, *114*(11), 1690–1696. https://doi.org/10.1289/ehp.9266

Rocklov, J., Barnett, A. G., & Woodward, A. (2012). On the estimation of heat-intensity and heat-duration effects in time series models of temperature-related mortality in Stockholm, Sweden. *Environmental Health*, *11*, 23. https://doi.org/10.1186/1476-069X-11-23

Russo, S., Sillmann, J., & Sterl, A. (2017). Humid heat waves at different warming levels. *Scientific Reports*, *7*(1), 7477. https://doi.org/10.1038/s41598-017-07536-7

Schnell, J. L., & Prather, M. J. (2017). Co-occurrence of extremes in surface ozone, particulate matter, and temperature over eastern North America. *Proceedings of the National Academy of Sciences*, *114*(11), 2854–2859.

Sherwood, S., & Fu, Q. (2014). A drier future? *Science*, *343*(6172), 737–739. https://doi.org/10.1126/science.1247620

Sherwood, S. C. (2018). How important is humidity in heat stress?. *Journal of Geophysical Research: Atmospheres*, *123*. https://doi.org/10.1029/2018JD028969

Sherwood, S. C., & Huber, M. (2010). An adaptability limit to climate change due to heat stress. *Proceedings of the National Academy of Sciences*, *107*(21), 9552–9555.

Shi, Y., Gao, X., Xu, Y., Giorgi, F., & Chen, D. (2016). Effects of climate change on heating and cooling degree days and potential energy demand in the household sector of China. *Climate Research*, *67*(2), 135–149.

Stafoggia, M., Schwartz, J., Forastiere, F., & Perucci, C. A. (2008). Does temperature modify the association between air pollution and mortality? A multicity case-crossover analysis in Italy. *American Journal of Epidemiology*, *167*(12), 1476–1485. https://doi.org/10.1093/aje/kwn074

Stull, R. (2011). Wet-bulb temperature from relative humidity and air temperature. *Journal of Applied Meteorology and Climatology*, *50*(11), 2267–2269.

Tiwari, S., Srivastava, A. K., Bisht, D. S., Bano, T., Singh, S., Behura, S., et al. (2009). Black carbon and chemical characteristics of PM_{10} and $PM_{2.5}$ at an urban site of North India. *Journal of Atmospheric Chemistry*, *62*(3), 193–209.

Tiwari, S., Srivastava, A. K., Bisht, D. S., Parmita, P., Srivastava, M. K., & Attri, S. D. (2013). Diurnal and seasonal variations of black carbon and $PM_{2.5}$ over New Delhi, India: Influence of meteorology. *Atmospheric Research*, *125*, 50–62.

Turner, M. C., Krewski, D., Pope, C. A. III, Chen, Y., Gapstur, S. M., & Thun, M. J. (2011). Long-term ambient fine particulate matter air pollution and lung cancer in a large cohort of never-smokers. *American Journal of Respiratory and Critical Care Medicine*, *184*(12), 1374–1381. https://doi.org/10.1164/rccm.201106-1011OC

Van Oldenborgh, G., Philip, S., Kew, S., van Weele, M., Uhe, P., Otto, F., & AchutaRao, K. (2017). Extreme heat in India and anthropogenic climate change. *Natural Hazards and Earth System Sciences*, *107*, 1–23.

Van Vuuren, D. P., Edmonds, J., Kainuma, M., Riahi, K., Thomson, A., Hibbard, K., et al. (2011). The representative concentration pathways: An overview. *Climatic Change*, *109*(1-2), 5.

WHO (2005). Air quality guidelines—Global updates 2005. http://www.euro.who.int/__data/assets/pdf_file/0005/78638/E90038.pdf?ua=1

Wilby, R. L. (2008). Constructing climate change scenarios of urban heat island intensity and air quality. *Environment and Planning. B, Planning & Design*, *35*(5), 902–919.

Willers, S. M., Jonker, M. F., Klok, L., Keuken, M. P., Odink, J., van den Elshout, S., et al. (2016). High resolution exposure modelling of heatwave and air pollution and the impact on mortality. *Environment International*, *89*, 102–109.

Willett, K. M., & Sherwood, S. (2012). Exceedance of heat index thresholds for 15 regions under a warming climate using the wet-bulb globe temperature. *International Journal of Climatology*, *32*(2), 161–177.

Wu, X., Xu, Y., Kumar, R., & Barth, M. (2019). Separating emission and meteorological drivers of mid-21st-century air quality changes in India based on multiyear global-regional chemistry-climate simulations. *Journal of Geophysical Research: Atmospheres*, *124*, 13,420–13,438. https://doi.org/10.1029/2019JD030988

Xu, Y., & Lamarque, J. F. (2018). Isolating the meteorological impact of 21st century GHG warming on the removal and atmospheric loading of anthropogenic fine particulate matter pollution at global scale. *Earth's Future*, *6*, 428–440.

Xu, Y., Lamarque, J. F., & Sanderson, B. M. (2018). The importance of aerosol scenarios in projections of future heat extremes. *Climatic Change*, *146*(3-4), 393–406.

Yin, H., & Sun, Y. (2018). Detection of anthropogenic influence on fixed threshold indices of extreme temperature. *Journal of Climate*, *31*(16), 6341–6352.

Zaveri, R. A., Easter, R. C., Fast, J. D., & Peters, L. K. (2008). Model for Simulating Aerosol Interactions and Chemistry (MOSAIC). *Journal of Geophysical Research*, *113*, D13204. https://doi.org/10.1029/2007JD008782